Engineering Analysis with Boundary Elements 105 (2019) 194–206

Contents lists available at ScienceDirect

Engineering Analysis with Boundary Elements

journal homepage: www.elsevier.com/locate/enganabound

A hybrid time-domain half-plane FE/BE approach for SH-wave scattering of alluvial sites

A. Nohegoo-Shahvari [a], M. Kamalian [b,*], M. Panji [c]

[a] Department of Civil Engineering, Arak Branch, Islamic Azad University, Arak, Iran
[b] Geotechnical Engineering Research Center, International Institute of Earthquake Engineering and Seismology (IIEES), No. 26, Arghavan Street, North Dibajee, Farmanieh, Tehran, Iran
[c] Department of Civil Engineering, Zanjan Branch, Islamic Azad University, Zanjan, Iran

ARTICLE INFO

Keywords:
Site effects
Half-plane BEM
FEM
SH waves
Wave scattering and diffraction

ABSTRACT

In this paper, a hybrid time-domain half-plane finite element-boundary element method (FEM/BEM) is developed to analyze the arbitrarily shaped alluvial sites subjected to propagating vertically incident plane *SH*-wave. First, the model is decomposed into two parts, a closed alluvial domain and an open valley-shaped feature as the surrounding medium. The former part is modeled by a conventional FE approach and, a recently proposed half-plane BEM is successfully applied to prepare the model of the latter part. After satisfying the continuity conditions at the interface, the coupled equations are solved step-by-step in FE framework to obtain the unknown values. In the use of the method, the interface of the basin needs to be discretized by BE meshes. Finally, the prepared computer algorithm is validated by solving some practical examples. The results show that the models are very simple and, the formulation has the appropriate accuracy. Furthermore, due to the significant reduction of the boundary elements in the half-plane BEM compared to the full plane BEM, the duration of the analysis and error waves in this formulation decreased. Therefore, the proposed hybrid method can be easily used in the nonlinear analysis of site response and the seismic interaction of soil-structure.

1. Introduction

Site effects typically lead to considerable damage on buildings close to topographic features after seismic events. For this reason, numerous methods have been introduced for modeling and quantitative definition of these effects. Among these methods, numerical ones, including volumetric, boundary, and hybrid methods have gained great attention.

In volumetric methods, as the first group of numerical methods, the domain of study area is discrete and the governing boundary conditions such as radiation of waves in the infinite are considered by defining approximate energy absorbing boundaries around the target area [1]. The most well-known volumetric methods are FEM, finite difference method (FDM) and spectral finite element method (SFEM). Many studies have been conducted on the seismic response of topographic features using these methods [2–10]. They are powerful tools to perform dynamic analysis on the finite plastic-elastic domains, however, their accuracy is reduced in the modeling of the infinite and semi-infinite domain and deal with some limitation; therefore, researchers have tried to use a numerical method such as BEM.

The BEM methods are basically developed for the purpose of analyzing the linear elastic domain, they can provide an opportunity for the user to evaluate the problem using the geometric boundary meshing of the domain. Providing the automatic radiation conditions of waves in an infinite domain is one of the most important advantages of this method. The BEM has been developed in two domains of time and frequency, but the advantages of combining with other numerical methods and analyzing various problems involving time dependent geometries and extracting real response values are possible only in time domain BEM. Several researchers have tried to improve the formulation of time-domain BEM and provide displacement and traction of the kernel for solving elastodynamic problems inside and outside the plane. Nevertheless, due to applying the Heaviside functions in the extraction of the kernel, the results have been reported in different waveforms by a reduction in the accuracy of the traction kernels [11–15]. To deal with this problem, Israil and Banerjee [16,17], without considering of Heaviside functions, presented full plane kernels for antiplane elastodynamics as the most accurate and precise results. Later, Kamalian et al. [18] modified the in-plane kernels and implemented them in the time-domain of the BEM algorithm to analyze seismic geotechnical problems [19–21]. Yu et al. [22] and Soares Jr et al. [23] modified the formulation of BEM in time-domain for out-of-plane elastodynamic problems. Sohrabi-Bidar et al. [24–26] performed a seismic analysis on 3D topographic features by

* Corresponding author.
E-mail addresses: a.nohegoo92@iau-arak.ac.ir (A. Nohegoo-Shahvari), Kamalian@iiees.ac.ir (M. Kamalian), m.panji@iauz.ac.ir (M. Panji).

https://doi.org/10.1016/j.enganabound.2019.04.020
Received 21 December 2018; Received in revised form 22 March 2019; Accepted 22 April 2019

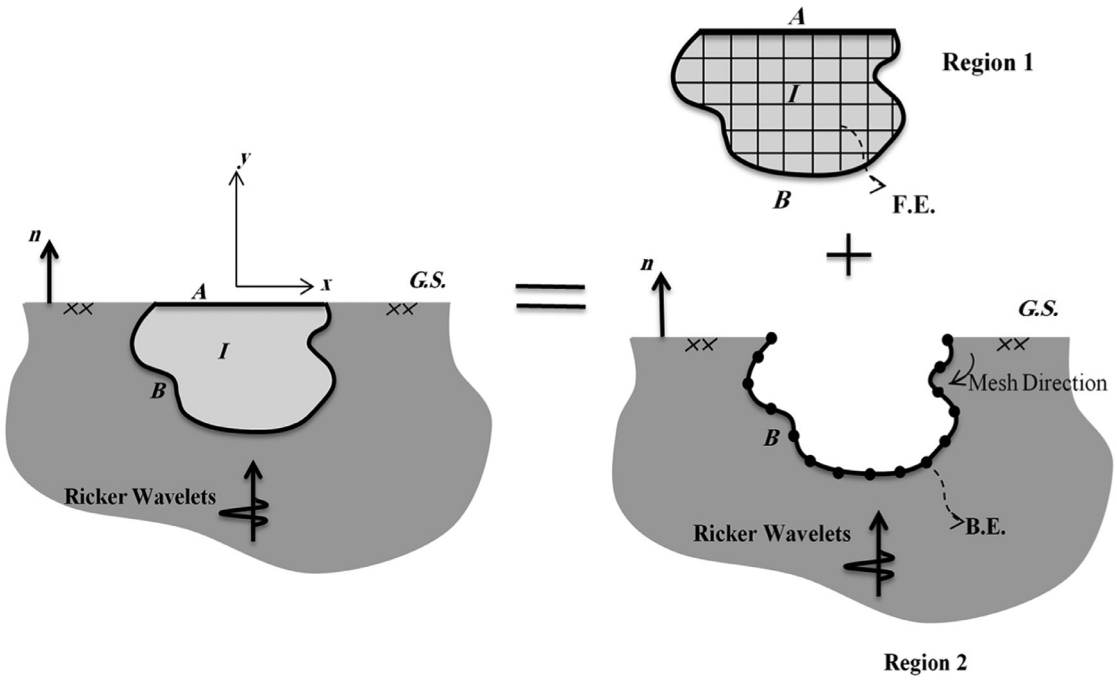

Fig. 1. Schematic design of the bounded region of FEM and unbounded region of BEM.

presenting elastodynamic traction kernels using BEM in time-domain. Recently, Panji et al. [27] presented a BEM in time domain along with closes and compressed complex half-plane time convoluted kernels. In this method, some parts of the feature that were higher than the ground surface were modeled. It is of note that this method takes the attention toward the seismic behavior of concave and convex topographies [28–30].

Takemiya and Fujiwara [31] were the first who evaluated the seismic motion of valleys and alluvial sites subjected to propagating incident SH waves in the time domain BEM. Then, Fishman and Ahmad [32] studied the dispersion of SH, SV, and P waves from semi-elliptical valleys employing BEM. Also, Semblat [33] evaluated local geological effects on site by the same method. Dravinski [34] employed indirect BEM to analyze the seismic response of alluvium with the folded middle base under propagating incident SH waves. Delépine and Semblat [35] and Kham et al. [36] respectively employed BEM to evaluate the seismic motion of high-height deep valley and deep alluvial basin in Tunisia. In recent years, Fu et al. [37,38] presented the method of the Singular boundary element as a simple mathematical approach and an easy program for analyzing the canyon topography.

The third group of numerical methods is Hybrid methods. Researchers often combine different numerical and analytical methods to enjoy the advantages of both of them, which lead to hybrid models. These methods can be divided into two groups. In the first group, the BEM is present as the basic method [39], but in the second group, other numerical or analytical methods for combining are used [40–42]. In the first group, the BEM are often combined with volumetric methods, which one of the most important advantages of this method is to provide a dynamic analysis of infinite plastic-elastic media in the time domain. Accordingly, dynamic analysis of infinite plastic-elastic media and infinite linear media around topographic feature are done using volumetric and boundary approaches, respectively. After publishing the hybrid BEM/FEM programs, which is suitable for time-domain simulations, Karabalis and Beskos [43] and Spyrakos & Beskos [44] employed them to evaluate the interaction of soil and structure in two dimensional and three-dimensional space. Based on their formulation, Von Estorff and Prabucki [45] presented a more comprehensive hybrid method for elastodynamic problems. Bielak et al. [46] also applied a hybrid BEM/FEM to evaluate the seismic response of homogeneous semicircular valleys subjected to incident SH waves. Later, Von Estorff and Firuziaan [47,48] developed this method to analyze the non-linear problems of soil and structure interaction. Kamalian et al. [49] presented a 2D non-linear hybrid BEM/FEM in time domain, which was implemented in the analysis of nonlinear and linear waves propagation [50–56]. Recently, Romero et al. [57] proposed a three-dimensional nonlinear method of combining FEM and BEM for solving soil and structure interaction problems. In this method, the FEM formulation was performed based on Green's implicit functions and nonlinear behavior at the interface of two methods was considered.

Therefore, the efficiency and accuracy of hybrid methods have led the authors of this paper to present a general algorithm in the time domain via combining the FEM and one of the novel methods of BEM called the half-plane BEM [27]. This BEM reduces the complexity of the model and the number of the boundary for meshing, and significantly reduces the duration of the analysis owing to discretization of some parts of the topographic feature [27]. Accordingly, in the present study, the alluvial site is decomposed into two domains. The first domain includes a closed alluvial domain modeled by the conventional FEM. The second domain is an open valley-shaped feature as the surrounding medium that the half-plane BEM is proposed for modeling. Then, to meet the boundary conditions at the interface, boundary stresses in the half-plane BEM are converted to node forces equivalent to FEM. Subsequently, the equations are solved in the framework of FEM to calculate the unknown values. Finally, a software is provided to implement this method in computer codes, and the accuracy of this method is examined using various examples.

2. Statement of the problem

In this section, the formulation of the problem and its matrix form are presented. As shown in Fig. 1, the study domain consists of two different regions. Region 1 is bounded and modeled by FEM. The boundaries of this region are the outer boundary A, which is the free surface of the ground, the internal boundary B is common with the boundary Region 2, and the internal points of this region are represented by the letter I. Region 2 is unbounded and modeled using the half-plane BEM. The

boundaries of this region are denoted as B boundary that is common with Region 1 and just this boundary of the feature gets mesh in the half-plane BEM. The governing equation on this problem is the differential (scalar wave) equation (Eq. (1)), which is presented for an isotropic, elastic, homogeneous domain with a small displacement domain [58] and the boundary condition governing on a linear and homogeneous elastic half-plane media is in accordance with Eq. (2).

$$\nabla^2 \tilde{u} + F = \frac{1}{c^2}\frac{\partial^2 \tilde{u}}{\partial t^2} \tag{1}$$

$$\mu \left.\frac{\partial \tilde{u}(x,y,t)}{\partial n}\right|_{y=0} = 0 \tag{2}$$

where $\tilde{u}$ is out-of-plane displacement, c is shear wave velocity equals to $\sqrt{\frac{\mu}{\rho}}$, ρ is density, μ is shear modulus, F is an out-of-plane volumetric force and, n is the normal vector which is perpendicular to the ground surface

2.1. Formulation of FEM

In the FEM, first, the weak formulation of Eq. (1) is extracted using weighed residues by Eq. (3).

$$\int_\Gamma q_i \delta\tilde{u}_i d\Gamma - \int_\Omega \tilde{\sigma}_{ij}\delta\tilde{\varepsilon}_{ij} d\Omega + \int_\Omega F_i \delta\tilde{u}_i d\Omega = \int_\Omega \rho\ddot{\tilde{u}}_i \delta\tilde{u}_i d\Omega \tag{3}$$

where $\tilde{\sigma}_{ij}$ and $\tilde{\varepsilon}_{ij}$ are respectively stress and strain tensor components in Ω an enclosed area (region 1) and q_i is traction on Γ boundary (boundary of region 1).

Then, Ω (the enclosed area) is divided into β numbers of small elements and elements of displacement, strain, and stress are defined as a function of displacement in each point of the node.

$$\begin{aligned}\tilde{u}^\beta &= L^\beta u^\beta \\ \tilde{\varepsilon}^\beta &= B^\beta u^\beta \\ \tilde{\sigma}^\beta &= C^\beta \tilde{\varepsilon}^\beta\end{aligned} \tag{4}$$

where $\mathbf{L}^\beta$, B^β, and C^β respectively are interpolation functions of displacement, strain-displacement matrices, and an elastic matrix of β the element. By replacing Eq. (4) in Eq. (3) the following equation is obtained:

$$\begin{aligned}&\sum_\beta \int_{\Gamma_\beta} q_i^\beta \delta\tilde{u}_i^\beta d\Gamma_\beta - \sum_\beta \int_{\Omega_\beta} \tilde{\sigma}_{ij}^\beta \delta\tilde{\varepsilon}_{ij}^\beta d\Omega_\beta + \sum_\beta \int_{\Omega_\beta} F_i^\beta \delta\tilde{u}_i^\beta d\Omega_\beta \\ &= \sum_\beta \int_{\Omega_\beta} \rho\ddot{\tilde{u}}_i^\beta \delta\tilde{u}_i^\beta d\Omega_\beta\end{aligned} \tag{5}$$

And, each term of Eq. (5) can be expressed by u vector as follows:

$$\begin{aligned}\int_{\Gamma_\beta} q_i^\beta \delta\tilde{u}_i^\beta d\Gamma_\beta &= \delta u^T \int_{\Gamma_\beta} L^{\beta T} q^\beta d\Gamma_\beta \\ \int_{\Omega_\beta} \tilde{\sigma}_{ij}^\beta \delta\tilde{\varepsilon}_{ij}^\beta d\Omega_\beta &= \delta u^T \int_{\Omega_\beta} B^{\beta T} C^\beta B^\beta d\Omega_\beta u \\ \int_{\Omega_\beta} F_i^\beta \delta\tilde{u}_i^\beta d\Omega_\beta &= \delta u^T \int_{\Omega_\beta} L^{\beta T} F^\beta d\Omega_\beta \\ \int_{\Omega_\beta} \rho\ddot{\tilde{u}}_i^\beta \delta\tilde{u}_i^\beta d\Omega_\beta &= \delta u^T \int_{\Omega_\beta} L^{\beta T} \rho L^\beta d\Omega_\beta \ddot{u}\end{aligned} \tag{6}$$

By substituting the definitions in Eq. (6) in Eq. (5) and after removing δu^Tcoefficient, the matrix form of the governing equation is obtained (Eq. (7)).

$$\mathbf{M}\ddot{\mathbf{u}} + \mathbf{K}\mathbf{u} = \mathbf{R} \tag{7}$$

where $\mathbf{M}$ is a mass matrix, $\mathbf{K}$ is the stiffness matrix, and $\mathbf{R}$ is the sum of surface and volumetric forces [10,59].

$$\begin{aligned}\mathbf{M} &= \sum_\beta M^\beta = \sum_\beta \int_{\Omega_\beta} L^{\beta T} \rho L^\beta d\Omega_\beta \\ \mathbf{K} &= \sum_\beta K^\beta = \sum_\beta \int_{\Omega_\beta} B^{\beta T} C^\beta B^\beta d\Omega_\beta \\ \mathbf{R} &= \sum_\beta \left(\int_{\Gamma_\beta} L^{\beta T} q^\beta d\Gamma_\beta + \int_{\Omega_\beta} L^{\beta T} F^\beta d\Omega_\beta \right)\end{aligned} \tag{8}$$

2.1.1. Time stepping algorithm

Among several methods to solve differential equations, in this paper, the Newmark's integration method is used. In this method, which is considered as the expansion of the linear acceleration method, the velocity and displacement are assumed in the form of Eq. (9), where α and δ are respectively considered to be 0.25 and 0.5 to supply integration accuracy and stability [60].

$$\begin{aligned}\left\{\dot{\mathbf{u}}^{t+\Delta t}\right\} &= \left\{\dot{\mathbf{u}}^t\right\} + \left[(1-\delta)\left\{\ddot{\mathbf{u}}^t\right\} + \delta\left\{\ddot{\mathbf{u}}^{t+\Delta t}\right\}\right]\Delta t \\ \left\{\mathbf{u}^{t+\Delta t}\right\} &= \left\{\mathbf{u}^t\right\} + \left\{\dot{\mathbf{u}}^t\right\}\Delta t + \left[\left(\frac{1}{2}-\alpha\right)\left\{\ddot{\mathbf{u}}^t\right\} + \alpha\left\{\ddot{\mathbf{u}}^{t+\Delta t}\right\}\right]\Delta t^2\end{aligned} \tag{9}$$

By re-writing Eq. (7) at time $(t+\Delta t)$ and substituting Eq. (9) in it, Eq. (10) is obtained for FEM governing the enclosed region:

$$\mathrm{K}_{FE}\cdot\left\{\mathbf{u}_{FE}^{t+\Delta t}\right\} = \mathbf{R}_{FE}^{t+\Delta t} + \mathbf{Z}_{FE}^{t+\Delta t} \tag{10}$$

Where

$$\begin{aligned}\mathbf{K}_{FE} &= \mathbf{K} + \frac{4}{\Delta t^2}\mathbf{M} \\ \mathbf{Z}_{FE}^{t+\Delta t} &= \mathbf{M}.\left(\frac{4}{\Delta t^2}\mathbf{u}^t + \frac{4}{\Delta t}\dot{\mathbf{u}}^t + \ddot{\mathbf{u}}^t\right) \\ \mathbf{R}_{FE}^{t+\Delta t} &= \mathbf{R}\end{aligned} \tag{11}$$

2.2. Half-plane BEM formulation

In BEM, the key parameters are determined by solutions obtained from the basic equation. The fundamental solutions of half-plane in the time domain can be determined by solving Eqs. (1) and (2). These solutions were presented by Panji et al. [27].

2.2.1. Boundary integration equations (BIE)

The main form of the equation of the direct boundary integral in the time domain can be obtained by applying the weighted residual integral to Eq. (1) and ignoring the contribution of the initial conditions and body forces. If the problem involves input waves, the BIE form is modified according to Eq. (12), as follows:

$$\begin{aligned}c(\xi)u(\xi,t) = &\int_\Gamma \left\{ \int_0^t \left[u^*(x,t;\xi,\tau).q(x,\tau) - q^*(x,t;\xi,\tau).u(x,\tau)\right] d\tau \right\} \\ &\times d\Gamma(x) + u^{ff}(\xi,t)\end{aligned} \tag{12}$$

where u^* and q^* respectively are the half-plane fundamental solutions for displacement and stress field in x point and t time induced by a unit anti-plane impulsive force at a point inξ location and preceding time of τ. Also, u and q are respectively boundary displacements and stresses, $\Gamma(x)$ is the boundary of the considered domain, $c(\xi)$ is geometric coefficient, and $u^{ff}(\xi,t)$ is displacement of the free field of the ground surface without irregular surfaces. To solve the BIE and to perform integrals, the axis of the time and the boundary of the domain must be discretized. Time integration can be obtained by discretization of time axis using N equal time steps with Δt duration ($t = N\Delta t$). Assuming a linear variable for the temporal interpolation functions, the BIE form is obtained as follows:

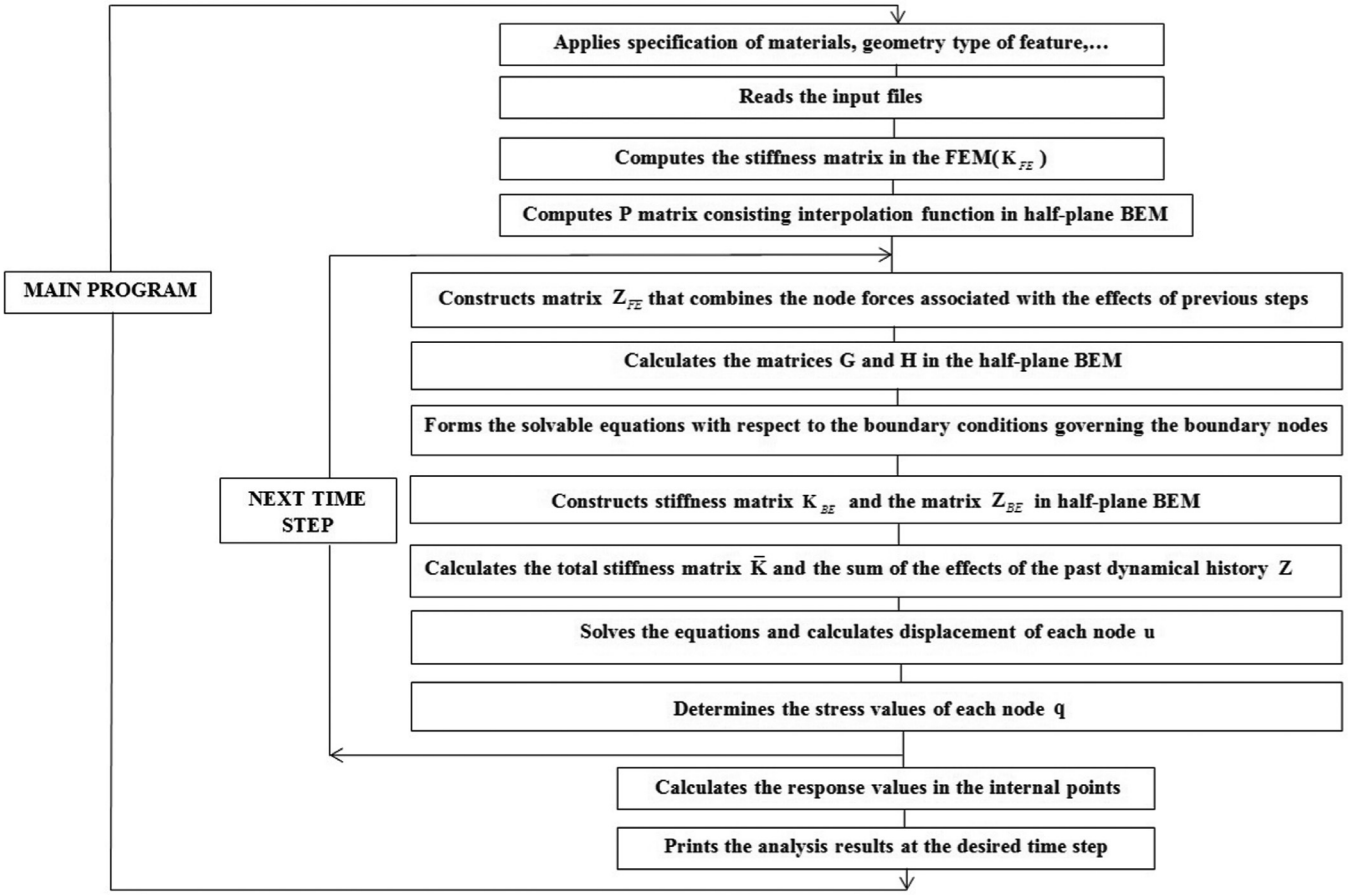

Fig. 2. The flowchart of the software.

$$c(\xi)u^N(\xi) = \sum_{n=1}^{N}\int_\Gamma \left(\begin{matrix}\left[U_1^{N-n+1}(x,\xi)+U_2^{N-n}(x,\xi)\right]q^n(x)-\\ \left[Q_1^{N-n+1}(x,\xi)+Q_2^{N-n}(x,\xi)\right]u^n(x)\end{matrix}\right) \times d\Gamma(x)+u^{f.N}(\xi) \tag{13}$$

where u^N and $u^{ff.N}$ are a boundary and free field displacement at $t=N\Delta t$, $U_1^{N-n+1}+U_2^{N-n}$ and $Q_1^{N-n+1}+Q_2^{N-n}$ are condensed closed-form of half-plane Scalar elastodynamic kernels for displacement and stress components, respectively, and $u^n(x)$ and $q^n(x)$ are respectively displacement and traction fields. All processes have been completely analyzed and half-plane scalar elastodynamic kernels have been provided by Panji et al. [27] for displacement and stress components. From now on, the approximation process is entered in the formulation considering the need for the discretization of the boundary of the domain to numerical integration of the location parameter in Eq. (13). For meshing the geometric boundary of the domain, a three-node second-order element is used and the spatial integral is numerically obtained as follows:

$$c(\xi)u^N(\xi) = \sum_{n=1}^{N}\sum_{\psi=1}^{\Psi}\left[\begin{matrix}\left\{\int_{\Gamma_\psi}\left[U_1^{N-n+1}(x(\kappa),\xi)+U_2^{N-n}(x(\kappa),\xi)\right]N_\alpha(\kappa)|J|d\kappa\right\}q_\alpha^n-\\ \left\{\int_{\Gamma_\psi}\left[Q_1^{N-n+1}(x(\kappa),\xi)+Q_2^{N-n}(x(\kappa),\xi)\right]N_\alpha(\kappa)|J|d\kappa\right\}u_\alpha^n\end{matrix}\right] + u^{f.N}(\xi) \tag{14}$$

where Ψ is the total number of boundary elements and Γ_ψ is a part of the boundary with element ψ being a part of it. $N_\alpha(\kappa)$ is quadratic shape functions in local intrinsic coordinates $\kappa(\alpha=1, 2, 3)$; u_α^n and q_α^n are respectively node values for displacement and stress; and J shows Jacobian of the transformation, which is obtained by regular and logarithmic Gaussian numerical integral for non-singular and singular integrals, respectively. The matrix form of BIE is obtained by Eq. (15) as follows [27]:

$$\sum_{n=1}^{N}\mathbf{H}^{N-n+1}\{\mathbf{u}^n\} = \sum_{n=1}^{N}\mathbf{G}^{N-n+1}\{\mathbf{q}^n\}+\{\mathbf{u}^{f.N}\} \tag{15}$$

where H^{N-n+1} and G^{N-n+1} are matrices obtained from the integration of half-plane kernels of stress and displacement on boundary elements. Also, u^n and q^n are vectors of node values of displacement and stress at the time step n. By writing Eq. (15) for each boundary node in $t+\Delta t$, the arrangement of the equation system takes the following matrix form.

$$\mathbf{H}^1.\mathbf{u}^N = \mathbf{G}^1.\mathbf{q}^N + \mathbf{Z}^N \tag{16}$$

where $\mathbf{u}^N$ and $\mathbf{q}^N$ are displacement and stress vectors and $\mathbf{Z}^N$ is the effects of dynamical history and displacement of the free field on the current time node N.

$$\mathrm{Z}^N = \sum_{n=1}^{N-1}\left(\mathbf{G}^{N-n+1}\{\mathbf{q}^n\}-\mathbf{H}^{N-n+1}\{\mathbf{u}^n\}\right)+\{\mathbf{u}^{f.N}\} \tag{17}$$

2.3. Combination of half-plane FEM/BEM

In FEM, governing equations are adjusted by displacement and node force, while in BEM they are adjusted by displacement and node stress. Therefore, these two methods should be compatible with each other to combine their governing equations. To deal with this issue, two methods are used: either converting equations of BEM to similar equations of FEM or converting the equations of FEM to similar equations of BEM. Considering that the first method has received much attention by researchers because of its efficiency in nonlinear analyses, it is used also in this paper. In order to adapt BEM to the FEM, boundary stresses must be converted to node forces equivalent to FEM. In doing so, both sides

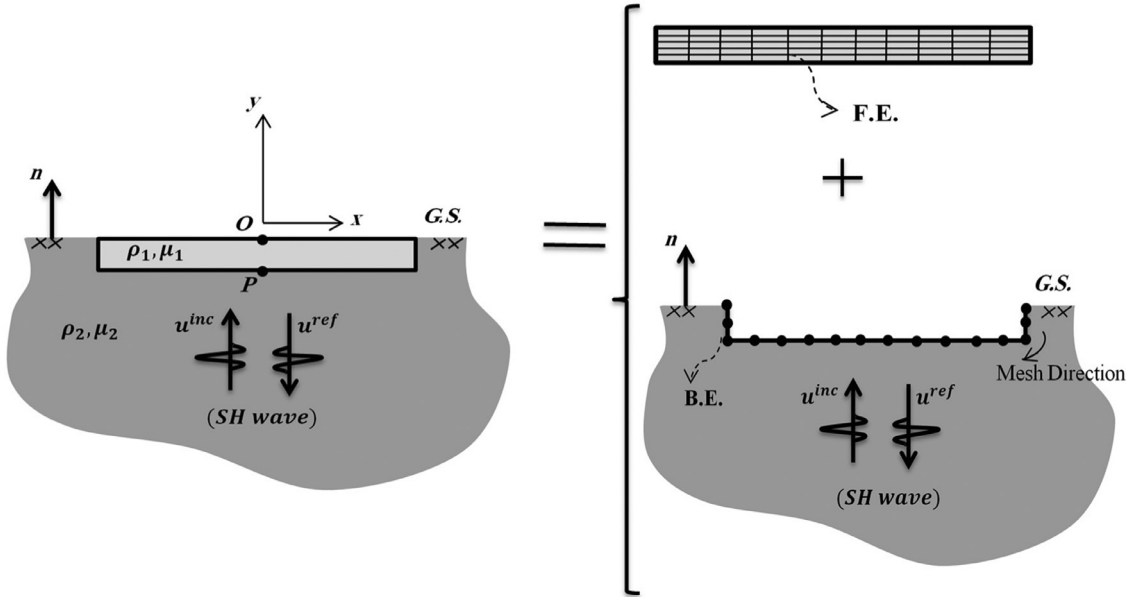

Fig. 3. The geometry of the one-dimensional site.

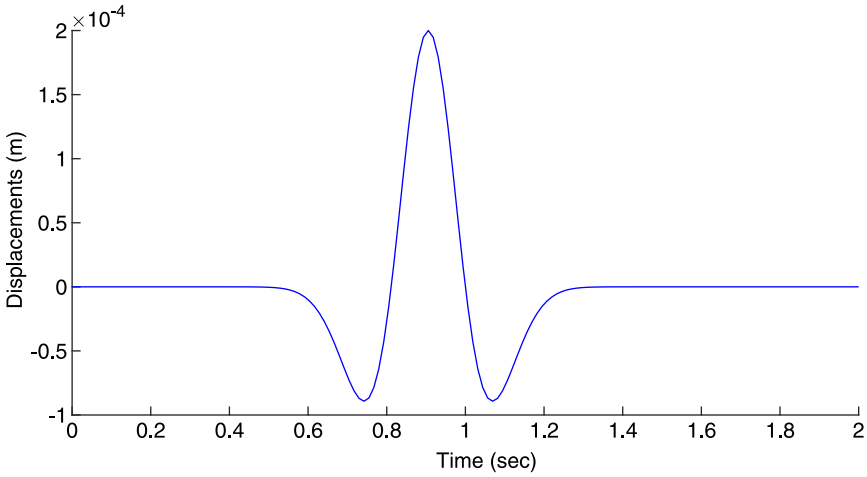

Fig. 4. The displacement time-history of input SH-wave in a point located in the flat surface of the ground in the time domain.

of Eq. (16) should be multiplied in reverse matrix $\mathbf{G}^1$ and then multiplied in the P matrix consisting of the interpolation functions used in the problem. As a result, the equation is obtained as follows [49,58]:

$$\mathbf{K}_{BE}.\left\{\mathbf{u}_{BE}^{t+\Delta t}\right\} = \mathbf{R}_{BE}^{t+\Delta t} + \mathbf{Z}_{BE}^{t+\Delta t} \tag{18}$$

where

$$\begin{aligned}
\mathbf{K}_{BE} &= \mathbf{P}.\mathbf{G}^{1^{-1}}.\mathbf{H}^1 \\
\mathbf{R}_{BE}^{t+\Delta t} &= \mathbf{P}.\mathbf{q}^N \\
\mathbf{Z}_{BE}^{t+\Delta t} &= \mathbf{P}.\mathbf{G}^{1^{-1}}.\mathbf{Z}^N \\
P^m &= \int_{\Gamma_m} N^T N d\Gamma_m
\end{aligned} \tag{19}$$

Based on Fig. 1, to connect finite element (FE) to boundary element (BE) region, the condition for compatibility of displacement and equilibrium should be provided. Therefore, the boundary condition in common boundary B is defined as follows:

$$\mathbf{u}_{FE}^B = \mathbf{u}_{BE}^B,\ \mathbf{R}_{FE}^B + \mathbf{R}_{BE}^B = 0 \tag{20}$$

Finally, the equation governing the bounded and unbounded regions is combined in $t+\Delta t$ time as follows:

$$\bar{\mathbf{K}}\mathbf{u}^{t+\Delta t} = \mathbf{R}^{t+\Delta t} + \mathbf{Z}^{t+\Delta t} \tag{21}$$

With respect to the regions defined in Fig. 1, the total stiffness matrix $\bar{\mathbf{K}}$, displacement vectors $\mathbf{u}^{t+\Delta t}$, force vectors $\mathbf{R}^{t+\Delta t}$, and the effects of the past dynamics history $\mathbf{Z}^{t+\Delta t}$ are defined as:

$$\begin{aligned}
\bar{\mathbf{K}} &= \begin{bmatrix} \mathbf{K}_{FE}^{AA} & \mathbf{K}_{FE}^{AI} & \mathbf{K}_{FE}^{AB} \\ \mathbf{K}_{FE}^{IA} & \mathbf{K}_{FE}^{II} & \mathbf{K}_{FE}^{IB} \\ \mathbf{K}_{FE}^{BA} & \mathbf{K}_{FE}^{BI} & \mathbf{K}_{FE}^{BB} + \mathbf{K}_{BE}^{BB} \end{bmatrix} \\
\mathbf{u}^{(t+\Delta t)^T} &= \begin{bmatrix} \mathbf{u}^A & \mathbf{u}^I & \mathbf{u}^B \end{bmatrix} \\
\mathbf{R}^{(t+\Delta t)^T} &= \begin{bmatrix} \mathbf{R}_{FE}^A & \mathbf{0} & \mathbf{0} \end{bmatrix} \\
\mathbf{Z}^{(t+\Delta t)^T} &= \begin{bmatrix} \mathbf{Z}_{FE}^A & \mathbf{Z}_{FE}^I & \mathbf{Z}_{FE}^B + \mathbf{Z}_{BE}^B \end{bmatrix}
\end{aligned} \tag{22}$$

After solving Eq. (21) and determining the unknown quantities in all nodes, one can determine the response of any internal point ψ in Region 2, such as the points of the ground surface around the desired feature (Eq. (23)).

$$\left\{\mathbf{u}^{N.\psi}\right\} = \sum_{n=1}^{N}\left(\mathbf{G}^{\langle N-n+1\rangle.\psi}\left\{\mathbf{q}^n\right\} - \mathbf{H}^{\langle N-n+1\rangle.\psi}\left\{\mathbf{u}^n\right\}\right) + \left\{\mathbf{u}^{ff.N.\psi}\right\} \tag{23}$$

where $\mathbf{G}^{\langle N-n+1\rangle.\psi}$ and $\mathbf{H}^{\langle N-n+1\rangle.\psi}$ are matrices with their elements derived from the integration of dynamically institutionalized half-plane

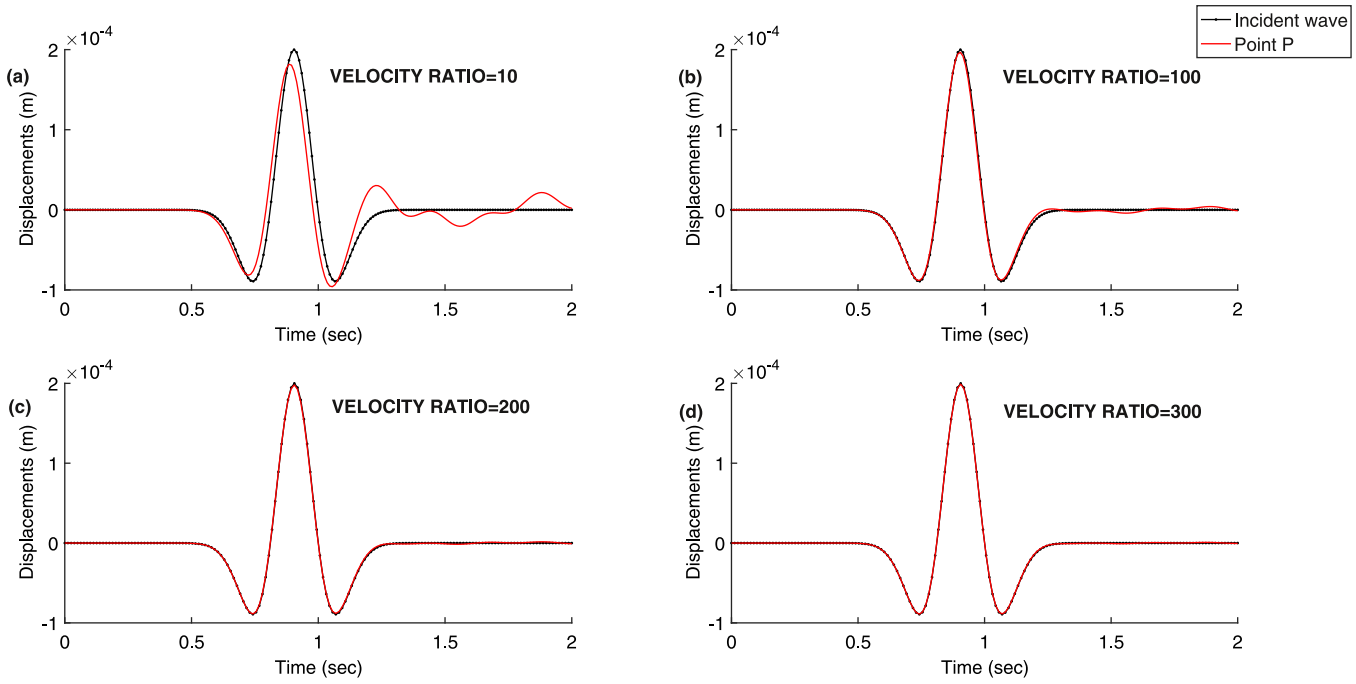

Fig. 5. The displacement time-history on the bottom boundary of site and comparison with displacement time-history of input SH-wave.

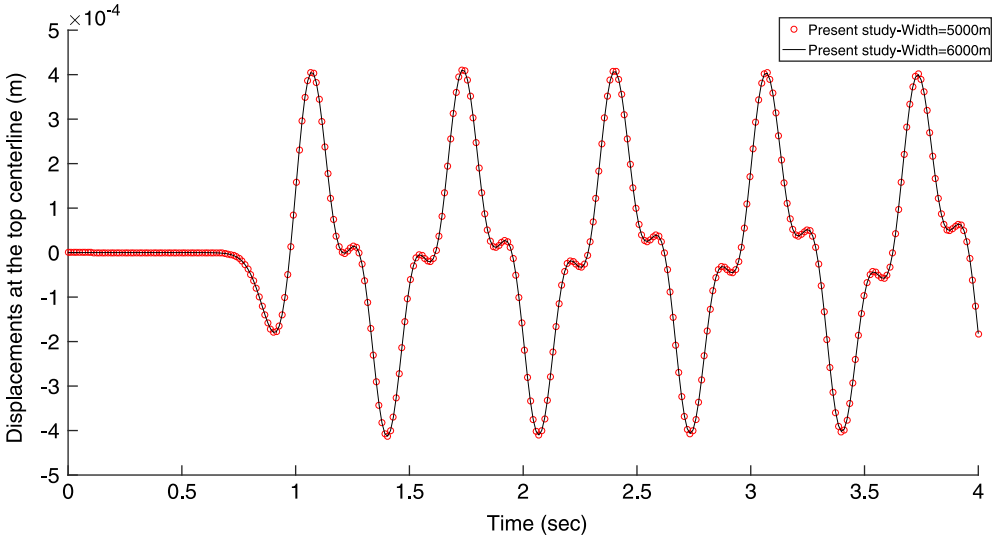

Fig. 6. The displacement time-history of the central point of the site on the ground surface (Point O).

elastodynamic kernels based on the position of the boundary nodes and the internal points. Moreover, $\mathbf{u}^{N.\psi}$ denotes the displacement values in internal points and $\mathbf{u}^{ff.N.\psi}$ denotes vectors including free movement of the ground surface in the internal points.

3. Flowchart

A software called DASFEBEM (Dynamic Analysis of Structure by Finite Element/Boundary Element Method) is prepared in MATLAB domain based on the formulation presented in Section 2. This software analyzes the dynamic response of the 2D domain under SH seismic wave by considering elastic behavior, and calculates deformation and stress. In FEM, 8-node elements and in BEM, second-order 3-node elements are used. All main subprograms are called as MAIN PROGRAM. In this section, the management of time steps and run of the program is performed. The subprograms, which are called by the MAIN PROGRAM command, are introduced by the order of calling (Fig. 2).

To evaluate the accuracy, efficiency, and capability of the aforementioned method for the analysis of topographic features in the time domain, four examples will be solved.

4. Validation examples

4.1. One-dimensional

In this example, the analysis of the response of a one-dimensional site with a homogeneous and uniform soil layer on rigid bedrock subjected to the propagation of vertical SH-wave is performed. As shown in Fig. 3, the problem is modeled as a rectangular alluvial valley located in a half-space media, where μ_1 and ρ_1 respectively are shear modulus and alluvial density and μ_2 and ρ_2 respectively are shear modulus and density of half-space. In this example, the selected radiant wave is Ricker wavelet function (Eq. (24)) [61,62].

$$F(t) = \left[1 - 2\left(\pi f_p(t - t_0)\right)^2\right] e^{-\left(\pi f_p(t-t_0)\right)^2} \tag{24}$$

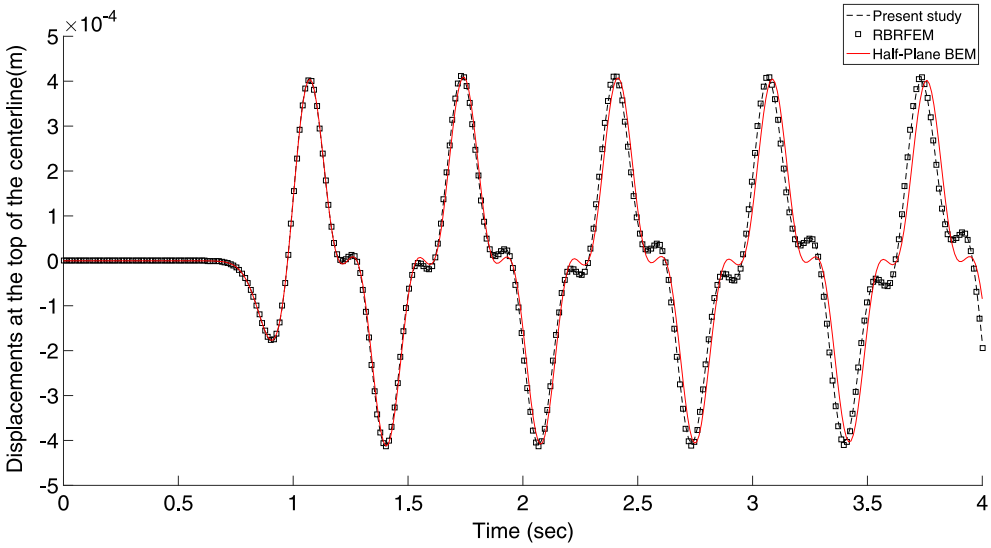

Fig. 7. The displacement time-history of the central point of the site on the ground surface with the present method, half-plane BEM and RBRFEM (Point O).

Table 1
The specification of material to supply rigid boundaries.

$\frac{c_2}{c_1}$	ρ_1 (t/m^3)	ρ_2 (t/m^3)	μ_1 (kN/m^2)	μ_2 (kN/m^2)	
10	2	2.1	180,000	189×10^5	1
100	2	2.1	180,000	189×10^7	2
200	2	2.1	180,000	756×10^7	3
300	2	2.1	180,000	1.701×10^{10}	4

Table 2
Site and input wave properties in the one-dimensional example.

A_{max} (m)	f_p(Hz)	t_0(s)	ρ_1 (t/m^3)	ρ_2 (t/m^3)	μ_1 (kN/m^2)	μ_2 (kN/m^2)
0.0001	2.4	0.9	2	2.1	180,000	1.701×1010

Table 3
Site specifications and input wave in a 2D example (a rectangular alluvial valley).

A_{max} (m)	f_p(Hz)	t_0(s)	ρ_1 (t/m^3)	ρ_2 (t/m^3)	μ_1 (kN/m^2)	μ_2 (kN/m^2)
0.001	3	1.7	1.4	2.1	126,000	756,000

Table 4
Site specifications and input wave in a 2D example (a semicircular alluvial valley).

A_{max} (m)	f_p(Hz)	t_0(s)	ρ_1 (t/m^3)	ρ_2 (t/m^3)	μ_1 (kN/m^2)	μ_2 (kN/m^2)
0.001	3	1.7	$\frac{2}{3}\rho_2$	2.1	$\frac{1}{6}\mu_2$	756,000

where f_p, t_0, and t respectively are the dominant frequency, time shift parameter, and time real axis. Based on Eq. (24), displacements of the free field of ground surface u^{ff} are calculated by Eq. (25).

$$u^{ff}(x,y,t) = u^{inc}(x,y,t) + u^{ref}(x,y,t) \tag{25}$$

where u^{inc} and α^{inc} respectively are displacement and the phase of incident wave in r^{inc} position and t time; u^{ref} and α^{ref} respectively are displacement and reflected wave phase from ground surface in the position of r^{ref} and time of t; A_{max} is the maximum displacement of time history; H is Heaviside function; and c is the velocity of the shear wave.

$$u^{inc}(x,y,t) = A_{max}\left[1-2\left(\frac{\pi f_p}{2}\alpha^{inc}\right)^2\right]e^{-\left(\frac{\pi f_p}{2}\alpha^{inc}\right)^2}H\left(t-\frac{r^{inc}}{c}\right)$$

$$u^{ref}(x,y,t) = A_{max}\left[1-2\left(\frac{\pi f_p}{2}\alpha^{ref}\right)^2\right]e^{-\left(\frac{\pi f_p}{2}\alpha^{ref}\right)^2}H\left(t-\frac{r^{ref}}{c}\right)$$

$$\alpha^{inc} = c(t-t_0) + r^{inc}$$

$$r^{inc} = -\sin\theta x + \cos\theta y$$

$$\alpha^{ref} = c(t-t_0) + r^{ref}$$

$$r^{ref} = -\sin\theta x - \cos\theta y \tag{26}$$

In order to model one-dimensional site, two issues should be considered: first, in this example, rigid boundary conditions should be provided so that the displacements of the time history of the points on the boundary are identical and in accordance with the motion of input shear waves. Second, the dimensions of the site should be chosen in a way that there is a sufficient distance between the lateral boundaries to prevent the error from the reflected waves at the central point of the ground surface.

To simulate rigid boundary conditions, a site with a width of 6000 m and a depth of 50 m is assumed, where the maximum displacement of time histories, dominant frequency, and time shift parameters are considered to be 0.0001 m, 2.4 Hz, and 0.9 s, respectively (Fig. 4). Next, several shear wave ratios are tested between half-space and alluvial materials ($\frac{c_2}{c_1}$). This test is carried out to the extent that the results of the displacement of the time history of the point on the boundary match with the displacement of the time history of the input wave. Table 1 presents the specifications of the materials and the tests list.

To compare the results of the test, point P is selected on the bottom boundary of the site (Fig. 3). The results of displacement time-history of this point is shown in Fig. 5. As can be seen, an increase in the velocity ratio results in overlapping boundary point displacement on displacement time-history of input wave and, finally, in a velocity ratio of 300, the rigid boundary condition is met.

To determine the dimension of the one-dimensional site, the analysis results of two models with dimensions of 5000 m × 50 m and 6000 m × 50 m are compared, such that each model is meshed with 200 and 240 elements of 8 nodes in the FE and 104 and 124 elements of second-order 3-nodes in the BE. This analysis is conducted to select the sufficient distance between the lateral boundaries and to simulate the one-dimensional ground conditions. In this analysis, the time step is 0.0125 s and the number of the time step is assumed to be 320. In Fig. 6, the displacement time-history derived from the analysis of the

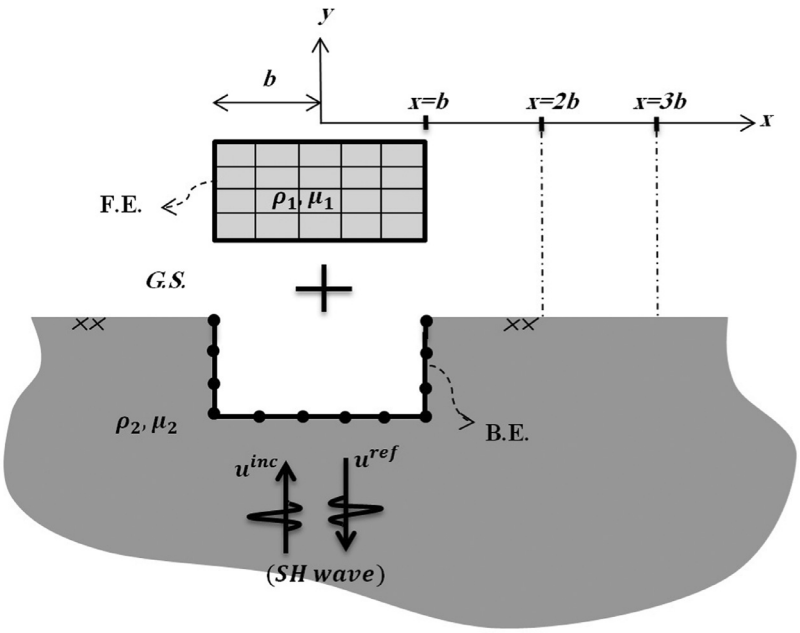

Fig. 8. The geometry and meshing of the 2D site (a rectangular section).

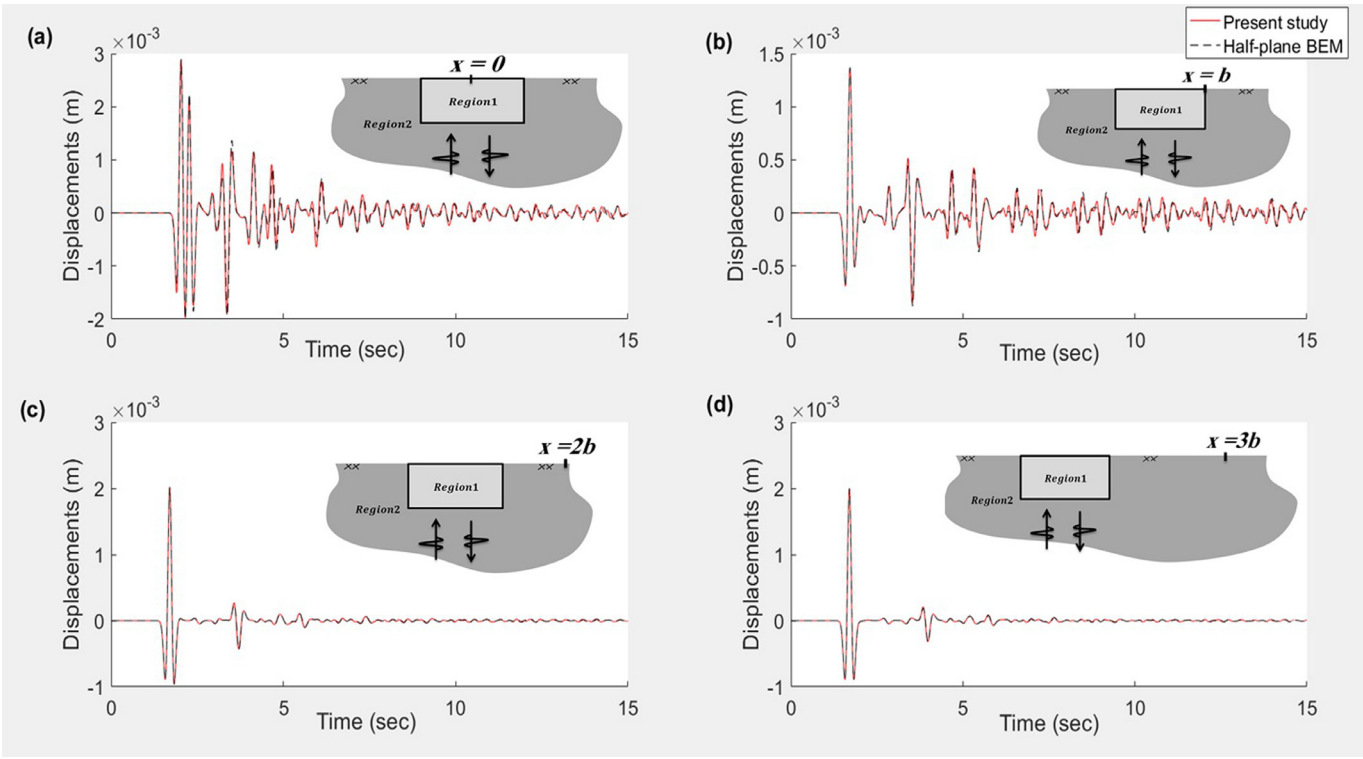

Fig. 9. The displacement time history of four-points on the ground surface with the present method and half-plane BEM.

two models are plotted on the central point on the ground surface. Two obtained curves overlap completely, indicating that the distance between the two lateral boundaries is sufficient to simulate the one-dimensional site. Then, the width of 6000 m was considered to analyze the one-dimensional site.

At this stage, as described in the above paragraph, a 6000 m × 50 m site is examined. In the analysis of this site, 240 8-node elements with 50 m × 25 m dimensions in FE area and 124 second-order 3-node elements are used in BE area (totally 965 nodes). The time step and the number of steps are assumed to be 0.0125 s and 320, respectively. In Table 2, the specifications of materials and input wave are presented.

To verify the obtained results, the half-plane BEM [27] and RBRFEM [10] is used and compared with the central point on the ground surface (point O). As shown in Fig. 7, there is a good agreement between the results of this point's displacement time-history in both methods. Another point that should be addressed in solving this problem is the confinement of wave in the valley in the very high-velocity ratio due to the action of the site as a cavity, which causes obtaining undamped results (Fig. 7).

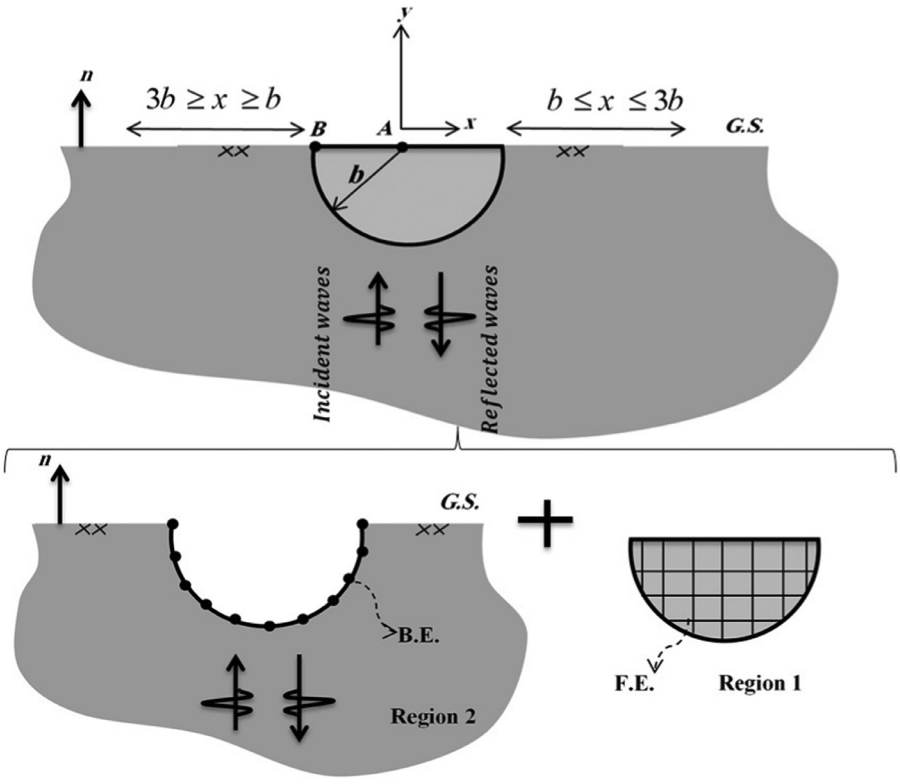

Fig. 10. The geometry of the two-dimensional site (a semicircular alluvial valley).

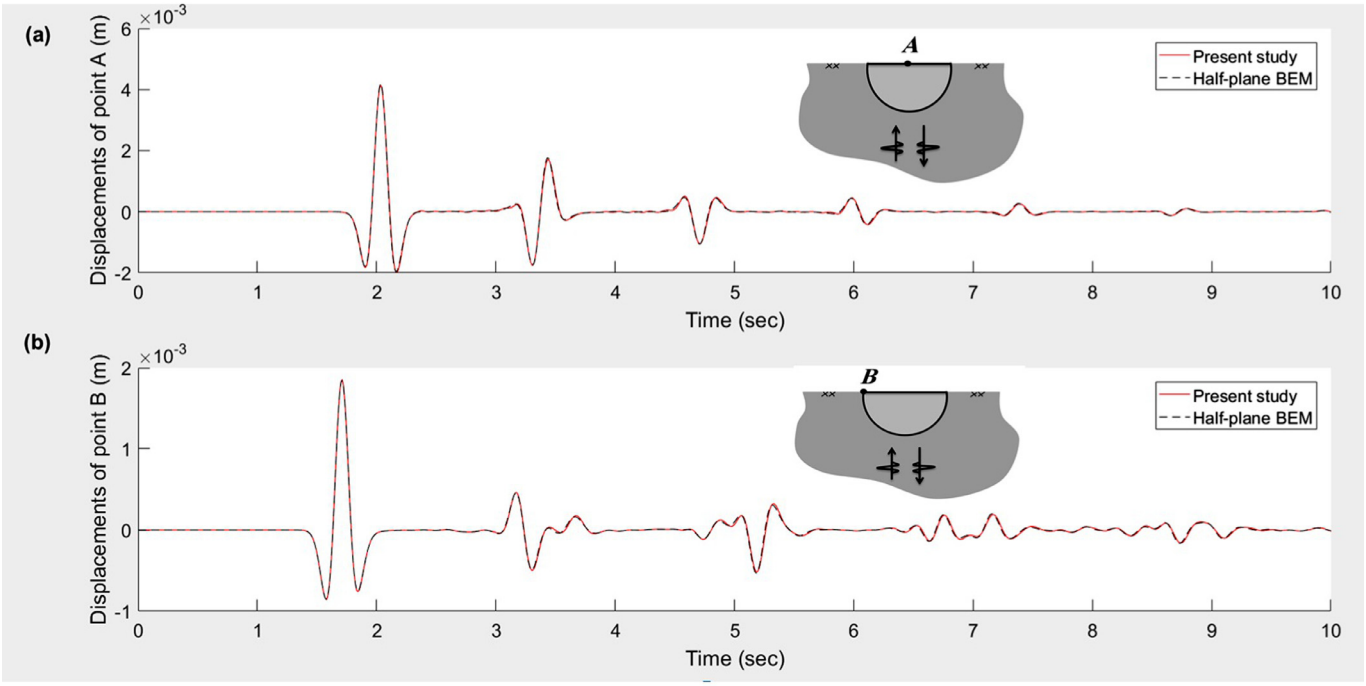

Fig. 11. Time-domain displacement of two points of the semi-circle alluvial valley: (a) top of the centerline (Point A); (b) edge of the valley (Point B).

4.2. A rectangular alluvial valley

In order to evaluate the efficiency and accuracy of this program in the analysis of two-dimensional problems, a rectangular 400 m × 200 m alluvial valley is analyzed in half-space. The soil layer assumed in this example is homogeneous and uniform, with characteristics presented in Table 3.

In the analysis of this site, 200 8-node elements with 20 m × 20 m dimensions in FE area and 40 second-order 3-node elements are used in BE area (totally 661 nodes). The time step and the number of steps are assumed to be 0.004 s and 3750, respectively. Fig. 8 shows the geometry and meshing of this site.

In this section, to validate the results, half-plane BEM [27] is used and the results are compared in 4 points on the ground surface ($x = 0$, b,

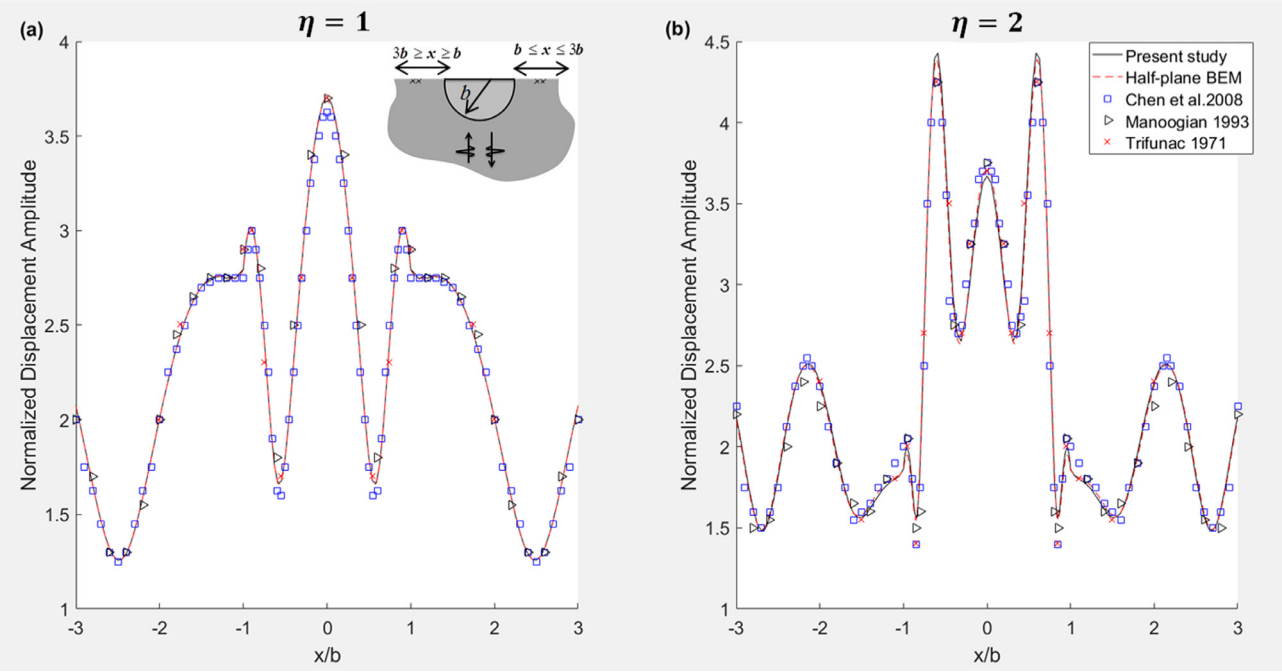

Fig. 12. Normalized displacement amplitude on the surface of the semi-circle alluvial valley and adjacent to it: (a) ($\eta = 1$) and (b) ($\eta = 2$).

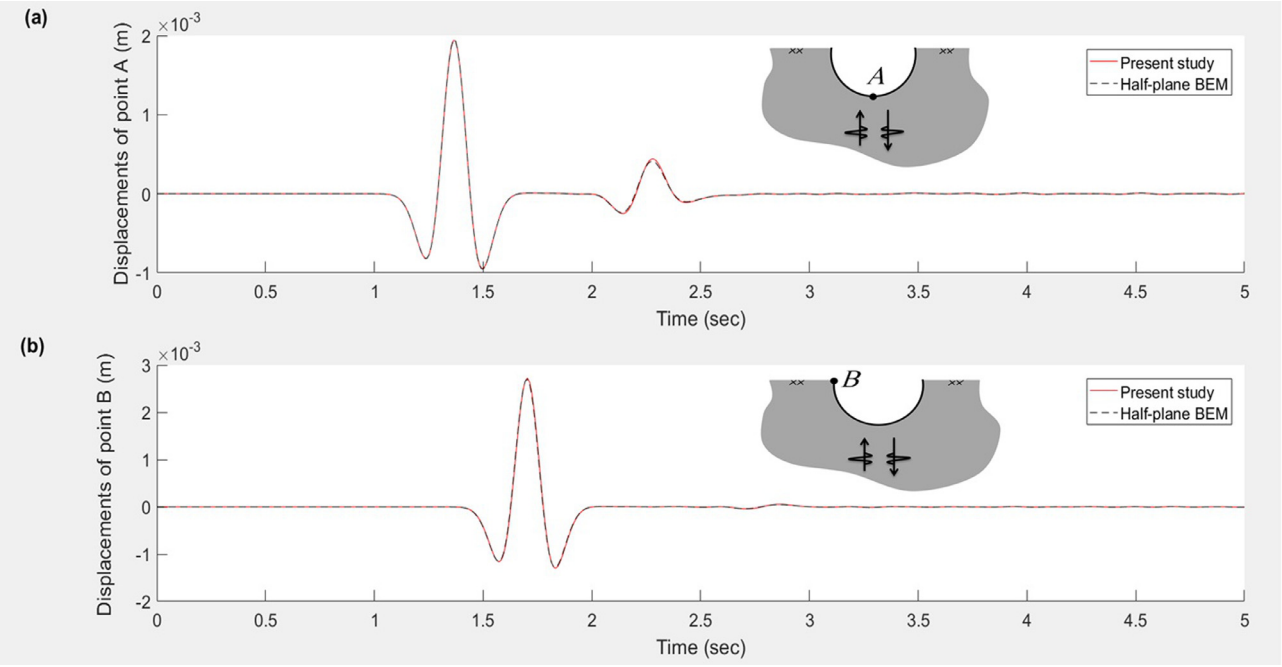

Fig. 13. Time-domain displacement of two points of the semi-circular canyon: (a) the canyon floor (Point A); (b) edge of the valley (Point B).

2b, 3b, where b is half width of the valley). As shown in Fig. 9, there is a good agreement between the results of the time history of these points in both methods.

4.3. A semicircular alluvial valley

In this two-dimensional example, a semicircular alluvial valley with a radius of 200 m, located in a half-space, is analyzed. The soil layer assumed in this example is homogeneous and uniform, with specifications presented in Table 4.

In the analysis of this site, 240 8-node elements in FE region and 60 second-order 3-node elements in BE region and a total of 811 nodes are used. The time step in problem-solving is 0.01 s. Fig. 10 presents the geometry and meshing of this site respectively.

In this section, the verifications of the results are done in two domains of time and frequency. In the time domain, the displacement time-history of the central point (A) and the valley edge (B) (Fig. 10) is compared to half-plane BEM [27], which shows a good agreement between the results (Fig. 11). To verify the accuracy in converted space, the dimensionless frequency $\eta = \frac{\omega b}{\pi c}$ is defined; where η is dimensionless frequency, ω is the angular frequency of the incident wave, c is the velocity of the shear wave, and b is the radius of the semi-circle. The normalized displacement amplitude of the site surface and its adjacent region is plotted in two non-dimensional frequencies 1 and 2 in Fig. 12.

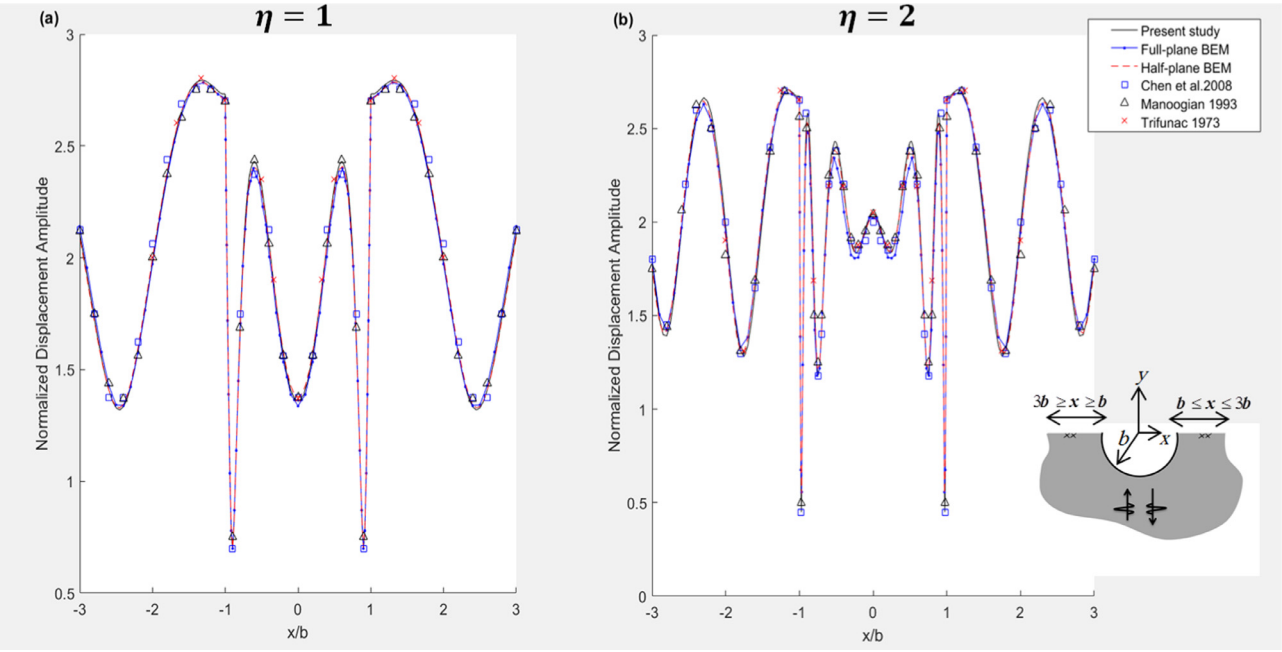

Fig. 14. Normalized displacement amplitude on the surface of the semi-circular canyon and adjacent to it: (a) ($\eta = 1$) and (b) ($\eta = 2$).

Table 5
The CPU times from executing time-domain half-plane FE/BE codes with an Intel (R) Core (TM) i5 CPU 7400 at 3.00 GHz and 16 GB RAM.

Examples	Dimensions (m)	Half-Plane FE/BE					Half-plane BEM	Full-plane BEM	
		The number of FEM elements	The number of the half - plane BEM elements	Time step (s)	Number of steps	Total time of analysis (s)	Total time of analysis (s)	The number of elements	Total time of analysis (s)
One-dimensional	W6000 × H50	240	124	0.0125	320	277.662	1648.075	–	–
Rectangular alluvial valley	W400 × H200	200	40	0.004	3750	1061.602	766.107	–	–
Semicircular alluvial valley	R200	240	60	0.01	1000	356.031	330.165	–	–
Semicircular canyon	R200	240	60	0.01	500	162.925	58.143	123	11,238.113

The *W* and *H* are the width and depth of the rectangular valley, respectively.
The *R* is the radius of the semicircular valley.

Normalized displacement amplitude is defined as the ratio of the Fourier amplitude of the total motion obtained by the hybrid method to the Fourier amplitude of the incident motion [29]. The obtained results are compared with the results presented by Trifunac [63], Manoogian [64], Chen et al. [65] and the half-plane BEM [27]. As can be seen, the results for both frequencies have a high accuracy.

4.4. A semicircular canyon

In this example, a semi-circular canyon with a radius of 200 is analyzed. In order to model the canyon, the shear modulus of region 1 is considered to be 10^8 times smaller than region 2($\mu_1 = \mu_2 \times 10^{-8}$) [65]. The rest of the materials and input wave specifications are assumed to be the same as Section 4.3. The results of this example are plotted in time and frequency domain. In the time domain, two points on the floor (A) and the edge (B) of the canyon are selected. Then, the displacement time-history of these points is calculated using the hybrid method and half-plane BEM [27], which as can be seen in Fig. 13, are completely overlapping.

In order to verify the results in the frequency domain, the normalized displacement amplitude of the canyon surface and its adjacent region is calculated in two non-dimensional frequencies 1 and 2. Then the obtained results are compared with the results presented by Trifunac [66], Manoogian [64], Chen et al. [65], the half-plane BEM [27] and full-plane BEM [27] in Fig. 14. As can be seen, there is an acceptable agreement between the results.

5. Analysis time

In this section, the half-plane FE/BE software is evaluated for the duration of the analysis of the issues. The CPU time for each of the examples is measured in seconds and is presented in Table 5.Then, To prove the efficiency of the present method, its analysis time is compared with the full-plane BEM [27] and half-plane BEM [27] for the semicircular canyon example. The results are added to the Table 5. As the results show, the duration of the analysis is desirable, which can be attributed to the reduction of the boundary elements due to the discretization of the only boundary of the feature using the half-plane BEM. This comparison is also performed for other examples using half-plane BEM [27], which shows that the present method has a good performance.

6. Conclusions

In the current paper, an advanced hybrid formulation (half-plane FE/BE) was presented by which the seismic behavior of homogeneous and heterogeneous topographic features were evaluated under SH waves. In this method, the topographic feature was divided into two bounded

and unbounded domains. The bounded domain involved alluvial materials and was modeled using the conventional FEM, which is a suitable method to model the finite domain. The unbounded domain involved valley-shaped feature in semi-space medium is modeled using the half-plane BEM. The advantages of the half-plane BEM are that only the basin interface needs to be meshed, thereby reducing the number of mesh elements and simplifying the model. Then, two methods were compatible for combining the governing equations, and the governing equations of the BEM were converted to FEM equations. Subsequently, the equations were solved in the framework of the FEM, and the unknowns were calculated. In the next step, the formulation was run in computer codes, and the accuracy, efficiency, and ability of this formulation were illustrated by analyzing the response of some different sites (a one-dimensional site, a two-dimensional rectangular alluvial site, the semi-circle alluvial valley and semi-circle canyon). The results were compared to those of the published works indicating that the models were very simple, and the present method had the accuracy and the appropriate duration of the analysis. This method can also be used as an efficient method for nonlinear analysis of the seismic response of alluvial sites and the seismic problems of soil-structure interaction due to the reduction of the boundary elements, consequently, reducing the program run-time and error waves.

References

[1] Eringen AC, Suhubi ES. Elastodynamics. Academic Press; 1975.
[2] Chuhan Z, Chongbin Z. Effects of canyon topography and geological conditions on strong ground motion. Earthq Eng Struct Dyn 1988;16(1):81–97.
[3] Zhao C, Valliappan S. Incident P and SV wave scattering effects under different canyon topographic and geological conditions. Int J Numer Anal Methods Geomech 1993;17(2):73–94.
[4] Sincraian MV, Oliveira CS. Nonlinear analysis of seismic behaviour of a valley using the finite element method. In: Proceedings of the 11th European conference on earthquake engineering, 559, Paris, Rotterdam. Balkema AA; 1998.
[5] Bielak J, Xu J, Ghattas O. Earthquake ground motion and structural response in alluvial valleys. J Geotech Geoenviron Eng 1999;125:413–23.
[6] Sincraian MV, Oliveira CS. Nonlinear seismic response of a volcanic hill using the finite element method. Soil Dyn Earthq Eng 2000;20(1–4):145–54.
[7] Chaljub E, et al. Spectral-element analysis in seismology. Adv Geophys 2007;48(7):365–419.
[8] Najafizadeh J, Kamalian M, Jafari MK, Khaji N. Seismic analysis of rectangular alluvial valleys subjected to incident SV waves by using the spectral finite element method. Int J Civ Eng 2014;12(3):251–63.
[9] Aminpour P, Najafizadeh J, Kamalian M, Jafari MK. Seismic response of 2D triangular-shaped alluvial valleys to vertically propagating incident SV waves. J Seismol Earthq Eng 2015;17(2):89–101.
[10] Nohegoo-Shahvari A, Kamalian M, Panji M. Two-dimensional dynamic analysis of alluvial valleys subjected to vertically propagating incident SH waves. Int J Civ Eng 2018.
[11] Cole DM, Kosloff DD, Minster JB. A numerical boundary integral equation method for elastodynamics. I. Bull Seismol Soc Am 1978;68(5):1331–57.
[12] Mansur WJ. Numerical implementation of the boundary element method for two dimensional transient scalar wave propagation problems. Appl Math Model 1982;6:299–306.
[13] Mansur WJ, Brebbia CA. Formulation of the boundary element method for transient problems governed by the scalar wave equation. Appl Math Model 1982;6(4):307–11.
[14] Mansur WJ. A time-stepping technique to solve wave propagation problems using the boundary element method. University of Southampton; 1983.
[15] Demirel V, Wang S. An efficient boundary element method for two-dimensional transient wave propagation problems. Appl Math Model 1987;11(6):411–16.
[16] Israil ASM, Banerjee PK. Advanced development of time-domain BEM for two-dimensional scalar wave propagation. Int J Numer Methods Eng 1990;29(5):1003–20.
[17] Israil ASM, Banerjee PK. Advanced time-domain formulation of BEM for two-dimensional transient elastodynamics. Int J Numer Methods Eng 1990;29(7):1421–40.
[18] Kamalian M, Gatmiri B, Sohrabi Bidar A. On time-domain two-dimensional site response analysis of topographic structures by BEM. J Seismol Earthq Eng 2003;5(2):35–45.
[19] Kamalian M, Gatmiri B, Sohrabi-Bidar A, Khalaj A. Amplification pattern of 2D semi-sine-shaped valleys subjected to vertically propagating incident waves. Commun Numer Methods Eng 2007;23(9):871–87.
[20] Kamalian M, Jafari K, Sohrabi-bidar A, Razmkhah A. Seismic response of 2-D semi–sine shaped hills to vertically propagating incident waves: amplification patterns and engineering applications. Earthq Spectra 2008;24(2):405–30.
[21] Kamalian M, Sohrabi-bidar A, Razmkhah A, Taghavi A, Rahmani I. Considerations on seismic microzonation in areas with two-dimensional hills. J Earth Syst Sci 2008;117(2):783–96.
[22] Yu G, Mansur WJ, Carrer JAM, Gong L. Stability of Galerkin and collocation time domain boundary element methods as applied to the scalar wave equation. Comput Struct 2000;74(4):495–506.
[23] Soares D Jr, Mansur WJ. An efficient time-truncated boundary element formulation applied to the solution of the two-dimensional scalar wave equation. Eng Anal Bound Elem 2009;33(1):43–53.
[24] Sohrabi-Bidar A, Kamalian M, Jafari MK. Time-domain BEM for three-dimensional site response analysis of topographic structures. Int J Numer Methods Eng 2009;79(12):1467–92.
[25] Sohrabi-Bidar A, Kamalian M, Jafari MK. Seismic response of 3-D Gaussian-shaped valleys to vertically propagating incident waves. Geophys J Int 2010;183(3):1429–42.
[26] Sohrabi-Bidar A, Kamalian M. Effects of three-dimensionality on seismic response of Gaussian-shaped hills for simple incident pulses. Soil Dyn Earthq Eng 2013;52:1–12.
[27] Panji M, Kamalian M, Marnani JA, Jafari MK. Transient analysis of wave propagation problrms by half-plane BEM. Geophys J Int 2013;194(3):1849–65.
[28] Panji M, Kamalian M, Marnani JA, Jafari MK. Antiplane seismic response from semi–sine shaped valley above embedded truncated circular cavity: a time-domain half–plane BEM. Int J Civ Eng 2014;12(2):193–206.
[29] Panji M, Kamalian M, Marnani JA, Jafari MK. Analysing seismic convex topographies by a half-plane time-domain BEM. Geophys J Int 2014;197(1):591–607.
[30] Panji M, Ansari B. Transient SH-wave scattering by the lined tunnels embedded in an elastic. Eng Anal Bound Elem 2017;84:220–30.
[31] Takemiya H, Fujiwara A. SH-wave scattering and propagation analyses at irregular sites by time domain BEM. Bull Seismol Soc Am 1994;84(5):1443–55.
[32] Fishman KL, Ahmad S. Seismic response for alluvial valleys subjected to SH, P and SV waves. Soil Dyn Earthq Eng 1995;14(4):249–58.
[33] Semblat JF, et al. Seismic wave amplification: basin geometry vs soil layering. Soil Dyn Earthq Eng 2005;25(7):529–38.
[34] Dravinski M. Scattering of waves by a sedimentary basin with a corrugated interface. Bull Seismol Soc Am 2007;97(1B):256–64.
[35] Delépine N, Semblat JF. Site effects in an alpine valley with strong velocity gradient: interest and limitations of the 'classical' BEM. Soil Dyn Earthq Eng 2012;38:15–24.
[36] Kham M, Semblat JF, Bouden-Romdhane N. Amplification of seismic ground motion in the Tunis basin: numerical BEM simulations vs experimental evidences. Eng Geol 2013;155:80–6.
[37] Fu Z, Chen W, Wen P, Zhang C. Singular boundary method for wave propagation analysis in periodic structures. J Sound Vib 2018;425(4):170–88.
[38] Tang Z, Fu Z, Zheng D, Huang J. Singular boundary method to simulate scattering of SH wave by the canyon topography. Adv Appl Math Mech 2018;10(4):912–24.
[39] Basnet MB, H Aji DB, Wuttke F, Dineva P. Wave propagation through poroelastic soil with underground structures via hybrid BEM-FEM. ZAMM Z Angew Math Mech 2018;98(8):1390–411.
[40] Chai Y, Li W, Gong Z, Li T. Hybrid smoothed finite element method for two-dimensional underwater acoustic scattering problems. Ocean Eng 2016;116:129–41.
[41] Chai Y, et al. Application of smoothed finite element method to two-dimensional exterior problems of acoustic radiation. Int J Comput Methods 2018;15(5):1850029.
[42] Shyu WS, Teng TJ, Chou CS. Anti-plane response induced by an irregular alluvial valley using a hybrid method with modified transfinite interpolation. Soil Dyn Earthq Eng 2016;90:250–64.
[43] Karabalis DL, Beskos DE. Dynamic response of 3-D flexible foundations by time domain BEM and FEM. Int J Soil Dyn Earthq Eng 1985;4(2):91–101.
[44] Spyrakos CC, Beskos DE. Dynamic response of flexible strip-foundations by boundary and finite elements. Soil Dyn Earthq Eng 1986;5(2):84–96.
[45] Von-Estorff O, Prabucki MJ. Dynamic response in the time domain by coupled boundary and finite elements. Comput Mech 1990;6(1):35–46.
[46] Bielak J, MacCamy RC, MacGhess DS, Barry A. Unified symmetric BEM-FEM for site effects on ground motion-SH waves. J Eng Mech 1991;117(10):2265–85.
[47] Von-Estorff O, Firuziaan M. Nonlinear dynamic response by coupling BEM and FEM. In: Proceeding of the ECCM99 conference, Munich; 1999.
[48] Von-Estorff O, Firuziaan M. Coupled BEM/FEM approach for nonlinear soil/structure interaction. Eng Anal Bound Elem 2000;24(10):715–25.
[49] Kamalian M, Jafari MK, Sohrabi-bidar A, Razmkhah A, Gatmiri B. Time-domain two-dimensional site response analysis of non-homogeneous topographic structures by a hybrid BE/FE method. Soil Dyn Earthq Eng 2006;26(8):753–65.
[50] Gatmiri B, Kamalian M. Two-dimensional transient wave propagation in anelastic saturated porous media by a Hybrid FE/BE method. In: Proc. 5th European conf. on numerical methods in geotechnical engineering; 2002. p. 947–56.
[51] Gatmiri B, Kamalian M, Karimi M, Sohrabi A. Seismic analysis of 2-dimensional response of canyons in time domain. In: Proceedings of the fourth international conference on seismology and earthquake engineering; 2003.
[52] Gatmiri B, Arson C, Nguyen KV. Seismic site effects by an optimized 2D BE/FE method I. Theory, numerical optimization and application to topographical irregularities. Soil Dyn Earthq Eng 2008;28(8):632–45.
[53] Gatmiri B, Arson C. Seismic site effects by an optimized 2D BE/FE method II. Quantification of site effects in two-dimensional sedimentary valleys. Soil Dyn Earthq Eng 2008;28(8):646–61.
[54] Gatmiri B, Foroutan T. New criteria on the filling ratio and impedance ratio effects in seismic response evaluation of the partial filled alluvial valleys. Soil Dyn Earthq Eng 2012;41:89–101.
[55] Gatmiri B, Amini-baneh D. Impact of geometrical and mechanical characteristics on the spectral response of sediment-filled valleys. Soil Dyn Earthq Eng 2014;67:233–50.
[56] Katebi M, Gatmiri B, Maghoul P. A numerical study on the seismic site response of rocky valleys with irregular topographic conditions. J Multiscale Model 2018:1850011.

[57] Romero A, Galvín P, Domínguez J. 3D non-linear time domain FEM-BEM approach to soil-structure interaction problems. Eng Anal Bound Elem 2013;37(3):501–12.
[58] Dominguez J. Boundary elements in dynamics. Boston: Wit Press; 1993.
[59] Desai CS, Christian JT. Numerical methods in geotechnical engineering. McGraw-Hill; 1979.
[60] Bathe KJ. Finite element procedures in engineering analysis. Englewood Cliffs, NJ: Prentice-Hall; 1982.
[61] Kawase H. Time-domain response of a semi-circular canyon for incident SV, P, and Rayleigh waves calculated by the discrete wavenumber boundary element method. Bull Seismol Soc Am 1988;78(4):1415–37.
[62] Ricker N. The form and laws of propagation of seismic wavelets. Geophysics 1953;18(1):10–40.
[63] Trifunac MD. Surface motion of a semi-cylindrical alluvial valley for incident plane SH waves. Bull Seismol Soc Am 1971;61(6):1755–70.
[64] Manoogian ME. Scattering and diffration of plane SH-waves by surdace and subsurface discontinuties. University Southern California; 1992.
[65] Chen JT, Chen PY, Chen CT. Surface motion of multiple alluvial valleys for incident plane SH-waves by using a semi-analytical approach. Soil Dyn Earthq Eng 2008;28(1):58–72.
[66] Trifunac MD. Scattering of PLane SH waves by a semi-cylinderical canyon. Earthq Eng Struct Dyn 1972;1(3):267–81.